ACS OMEGA

http://pubs.acs.org/journal/acsodf

Article

Relationship between Surface Hydroxyl Complexation and Equi-Acidity Point pH of MnO_2 and Its Adsorption for Co^{2+} and Ni^{2+}

Mingdong Li,[#] Jiawei Wang,[#] Bibo Gou, Dejin Fu, Haifeng Wang,[*] and Pingyuan Zhao

Cite This: *ACS Omega* 2022, 7, 9602−9613

Read Online

ACCESS | Metrics & More | Article Recommendations

ABSTRACT: MnO_2 has shown great potential in the field of adsorption and has a good adsorption effect on heavy metal ions in aqueous solution, but there have been problems in the adsorption of heavy metal ions in high-concentration metal salt solutions. In this paper, different crystal forms of MnO_2 (α-MnO_2, β-MnO_2, γ-MnO_2, δ_1-MnO_2, δ_2-MnO_2, and ε-MnO_2) were prepared and characterized by XRD, SEM, EDS, XPS, ZETA, and FT-IR. The reasons for the equi-acidity point pH change of MnO_2 and the complex mechanism of surface hydroxylation on metal ions were discussed. The results showed that the equi-acidity point pHs of different crystalline MnO_2 were different. The equi-acidity point pH decreased with the increase of reaction temperature and electrolyte concentration, but the reaction time had no effect on it. The equi-acidity point pHs of MnO_2 were essentially equal to the equilibrium pH values of adsorption and desorption between surface hydroxyl and metal ions on them. The change of equi-acidity points was mainly due to the complexation of surface hydroxyl, and the equi-acidity point pHs depended on the content of surface hydroxyl and the size of the complexation ability. According to the equi-acidity point pH characteristics of MnO_2, more hydroxyl groups could participate in the complexation reaction by repeatedly controlling the pH, so that MnO_2 could adsorb heavy metals Co^{2+} and Ni^{2+} in high-concentration $MnSO_4$ solution, and the adsorption rates of Co^{2+} and Ni^{2+} could reach 96.55 and 79.73%, respectively. The effects of MnO_2 dosage and Mn^{2+} concentration on the adsorption performance were further investigated, and the products after MnO_2 adsorption were analyzed by EDS and FT-IR. A new process for MnO_2 to adsorb heavy metals Co^{2+} and Ni^{2+} in high-concentration $MnSO_4$ solution was explored, which provided a reference for the deep purification of manganese sulfate solutions.

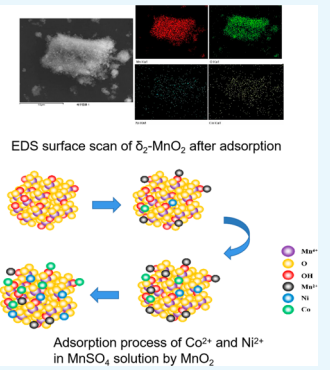

1. INTRODUCTION

MnO_2, as an environmentally friendly functional material, has been widely used in battery materials, molecular sieves, catalysis, and adsorption due to its wide range of sources, low cost, various morphologies, rich crystal forms, stable structure, and good physical and chemical properties.[1−5] The skeleton structure of MnO_2 was composed of a [MnO_6] octahedron sharing corners and edges. MnO_2 produced under different conditions had different crystal structures, such as α-MnO_2, β-MnO_2, γ-MnO_2, δ-MnO_2, ε-MnO_2, and λ-MnO_2. The surface physicochemical properties of MnO_2 with different crystal structures were quite different.[6] In addition, MnO_2 could be prepared into flower-like, rod-like, sea urchin-like, and other forms through different synthesis conditions.[7,8] MnO_2 had good adsorption properties due to its unique structural and morphological characteristics, high specific surface area, high porosity, abundant surface hydroxyl groups, and the large amount of surface charge.[9,10] In recent years, a large number of studies have been carried out on the application of MnO_2 in the removal of heavy metal ions. Good results have been achieved in adsorbing trace heavy metal ions Pb^{2+}, Cu^{2+}, Co^{2+}, Ni^{2+}, Zn^{2+}, and Cd^{2+} in water.[11−15] The adsorption properties of MnO_2 were greatly improved by calcination, doping, and modification.[16,17] The adsorption behavior was studied by researchers using advanced spectral analysis, a surface complexation model, and theoretical calculation; and the adsorption mechanism in aqueous solution has been well explained, usually involving ion exchange, electrostatic adsorption, hydrogen bonds, and surface complexes.[18,19] However, the adsorption of heavy metal ions in a metal salt solution has not been solved, the main reason being that a large number of metal ions hindered the adsorption, and there was a lack of in-depth discussion on the interaction between manganese dioxide and metal salt solution.[20]

Previously, many scholars found that solution pH would change when MnO_2 was mixed with an electrolyte solution with known pH, but the pH value of the solution would not change with addition of MnO_2 at a certain pH value, which was called the equi-acidity point pH.[21] The equi-acidity point pH varied with the crystal form of manganese dioxide, the composition of electrolyte solution, and the reaction conditions, which were

Received: December 8, 2021
Accepted: February 28, 2022
Published: March 9, 2022

© 2022 The Authors. Published by American Chemical Society

related to the surface hydroxyl adsorption and ion exchange properties of MnO_2.[22,23] Because there was no good analytical method or determination method at that time, the reasons for the change of equi-acidity point pH and the adsorption characteristics of surface hydroxylation on metal ions were not discussed in depth.

More attention had been paid to the influence of surface charge on the adsorption of MnO_2, so the isoelectric point and zero point charge of manganese dioxide were proposed, but the influence of surface defects and surface hydroxyl groups were less discussed.[24] Oxygen coordination around manganese vacancies was unsaturated due to defects, vacancies, and impurities in MnO_2, which would result in the presence of a large number of hydroxyl groups on the surface of MnO_2.[25] When heavy metal ions were adsorbed by MnO_2 in the form of surface hydroxyl complex, the solution pH was very important.[26] Therefore, the equi-acidity point pH values of different crystal MnO_2's were determined, the influencing factors were analyzed, the interaction between manganese dioxide and $MnSO_4$ solution was explored, and the surface hydroxyl complexation mechanism was analyzed, so as to further study the adsorption effect of MnO_2 surface hydroxylation on heavy metal ions. It would solve the problem of removing heavy metal ions from manganese sulfate solution, which was the raw material of manganese series batteries, and provide an impurity removal method for the preparation of high-purity manganese series materials.

2. EXPERIMENTAL SECTION

2.1. Reagents and Equipment. Analytically pure H_2SO_4, $KMnO_4$, $NH_4{\cdot}H_2O$, $(CH_3COO)_2Mn$, $NiSO_4{\cdot}6H_2O$, $CoSO_4{\cdot}7H_2O$, and $MnSO_4{\cdot}H_2O$ were provided by the Tianjin Kemio Company. A digital pH meter (PHS-25) was provided by the Shanghai Yidian Scientific Instrument Co., Ltd. A constant temperature drying oven (DHG-9005A) was provided by the Shanghai Yiheng Scientific Instrument Co., Ltd. A constant temperature water bath pot (HH-3), electric mixer (JJ-1), and vacuum suction filter pump (P4Z) were provided by the Shanghai Lichen Instrument Technology Co., Ltd., and an electronic analytical balance (PL2002) was provided by the METTLER TOLEDO group. The box resistance furnace (SX-4-10) was provided by the Tianjin Tester Instrument Co., Ltd. A cyclotron oscillator (HY-5B)was provided by the Changzhou Langyue Instrument Manufacturing Co., Ltd.

2.2. Selection and Preparation Process of MnO_2. In this experiment, α-MnO_2, β-MnO_2, γ-MnO_2, δ_1-MnO_2, δ_2-MnO_2, and ε-MnO_2 were chosen. α-MnO_2 was pure anode slag and was collected from a manganese production enterprise in Tongren, Guizhou. γ-MnO_2 was electrolytic manganese dioxide and was collected from a manganese production enterprise in Tongren, Guizhou. ε-MnO_2 was chemical manganese dioxide and was bought on the market. β-MnO_2 was prepared from the γ-MnO_2 of electrolytic manganese dioxide by heat treatment at 450 °C for 6 h. Two kinds of δ-MnO_2 with different morphologies were made by us in the laboratory.[27] δ_1-MnO_2 was prepared by using $(CH_3COO)_2Mn$ as manganese source, and δ_2-MnO_2 was prepared by using $MnSO_4{\cdot}H_2O$ as manganese source.

δ_1-MnO_2 was prepared in the following steps. After 300 mL of 0.1 mol/L potassium permanganate solution was stirred for 30 min, 150 mL of a 0.15 mol/L $(CH_3COO)_2Mn$ solution was added into it. When the reaction was completed at 80 °C for 6 h, the solution was cooled to room temperature and filtered to obtain a black precipitate. Then, the black precipitate was washed with deionized water for many times to remove impurity ions. Finally, it was dried at 100 °C for 12 h and became δ_1-MnO_2. Preparation of δ_2-MnO_2 was similar to that for δ_1-MnO_2. The only difference was that $(CH_3COO)_2Mn$ was replaced by manganese sulfate.

2.3. Characterization of MnO_2. The morphology and structure of MnO_2 were analyzed by a Hitachi SU8020 ultrahigh resolution field emission scanning mirror. XRD analysis was done using a D8 ADVANCE X-ray diffractometer of the Brooke company. FT-IR analysis was performed on the NICOLET IS 10 infrared spectrometer produced by Nigaoli, USA. XPS data were collected on a Thermo escalab 250Xi electronic spectrometer produced by Semerfeld, USA. Surface potential was measured by Zetasizer Nano ZS90 laser particle size analyzer produced by Semerfeld, USA.

2.4. Equi-Acidity Point pH Experiments. First, a manganese sulfate solution with Mn^{2+} concentration of 30 g/L was prepared. Then, 200 mL of it was put into 10 plastic bottles with a volume of 250 mL. Their pH values were asjusted to 0.5, 1, 1.5, 2, 2.5, 3, 3.5, 4, 4.5, and 5 with dilute sulfuric acid. Next, 2 g washed and dried MnO_2 was added into these $MnSO_4$ solutions. After being placed on a cyclotron oscillator and shaken for 12 h, the supernatant was taken out, and the pH value of each solution was measured by a pH meter. This procedure was repeated 6 times; the equi-acidity point pH of each different MnO_2 was obtained by plot analysis. Finally, the influence of reaction time, temperature, and Mn^{2+} concentration on the equi-acidity point pH of β-MnO_2 was explored.

2.5. Absorption Experiments. 500 mL manganese sulfate solution with Mn^{2+} concentration of 30 g/L and Ni^{2+} and Co^{2+} concentrations of 100 mg/L was prepared, the pH was adjusted to 7 with 10% ammonia, and 2 g MnO_2 was added. Then, it was put into a constant temperature water bath pot at 80 °C and stirred continuously. Due to the influence of the equi-acidity point pH of MnO_2, the pH of the solution would decrease to a certain value. The pH of the solution was adjusted to 7 by adding ammonia. With the reaction going on, the pH decreased again, and continued to be adjusted until the pH no longer decreased. The solution was filtered quickly, and the concentrations of Ni^{2+} and Co^{2+} in the filtrate were determined by an A3AFG-13 flame atomic absorption spectrometer. The adsorption rate of Ni^{2+} and Co^{2+} by MnO_2 was calculated by the following formula

$$Q = \frac{C_0 - C}{C_0} \times \% \quad (1)$$

In the formula, Q was the adsorption rate, C_0 was the initial concentration, and C was the concentration after adsorption.

3. RESULTS AND DISCUSSION

3.1. Characterization of MnO_2 with Different Crystal Forms. XRD characterization analysis of six different MnO_2 used in this study were shown in Figure 1. As can be seen from Figure 1, the anode slag of electrolytic manganese was mainly composed of α-MnO_2, with a small amount of MnOOH, PbO, and $(NH_4)_3Fe(SO_4)_3$. Its obvious peaks were at 2θ = 12.8°, 28.7°, 37.6°, and 65.7°, and they were in good agreement with the standard card (JCPDS-44-0141). Electrolytic MnO_2 belonged to γ-MnO_2 (according to standard card JCPDS-14-0644), and the 2θ diffraction peaks were prominent at 22.2°, 37.6°, 42.5°, and 56.2°. The γ-MnO_2 was completely transformed into β-MnO_2(according to standard card JCPDS-24-0735) after heat treatment at 450 °C for 5 h, and its 2θ

https://doi.org/10.1021/acsomega.1c06939
ACS Omega 2022, 7, 9602−9613

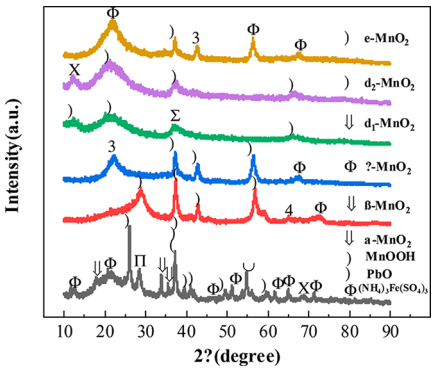

Figure 1. XRD patterns of MnO_2 with different crystal forms.

diffraction peaks were prominent at 28.6°, 37.3°, 42.8°, and 56.7°. Two kinds of δ-MnO_2 (δ_1-MnO_2, δ_2-MnO_2) prepared by manganese acetate and manganese sulfate had poor crystallinity; their characteristic peaks were at 2θ = 12.2°, 19.8°, 37.6°, and 65.7°; and they could better match the standard card JCPDS-18-0802. The main component of chemical MnO_2 was ε-MnO_2 (according standard card JCPDS-30-0820), and it had sharp absorption peaks at 21.1°, 37.4°, 42.5°, 56.3°, and 66.6°.

The morphology of MnO_2 with different crystal forms was shown in Figure 2. From the SEM images, it could clearly be

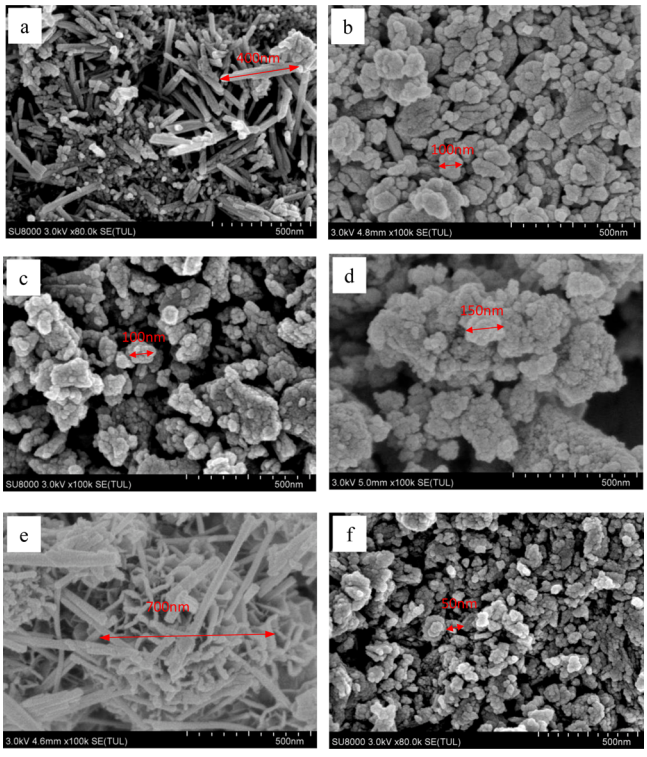

Figure 2. SEM images of MnO_2 with different crystal forms (a, α-MnO_2; b, β-MnO_2; c, γ-MnO_2; d, δ_1-MnO_2; e, δ_2-MnO_2; f, ε-MnO_2).

found that α-MnO_2 was generally nanorod-like with a length of about 400 nm. The nanorods were staggered and agglomerated with each other, and the gap was large, which would provide more surface hydroxyl sites, also providing conditions for the complexation of heavy metal ions. The ε-MnO_2, β-MnO_2, and γ-MnO_2 were spherical nanoparticles with different sizes. The crystal particles were small and dense, and the diameter was between 50 and 100 nm. The β-MnO_2 grains obtained by heat treatment were more dense than γ-MnO_2, which would lead to the surface hydroxyl only existing on the surface. So, the complexation reaction of heavy metal ions could only be carried out on the surface, and it could not take place in the internal structure. δ_1-MnO_2 was a layered structure with large voids formed by the accumulation of nanoflake particles with a diameter of about 150 nm. δ_2-MnO_2 was sea urchin-like, composed of nanorods with a diameter of about 700 nm, and had a rich pore structure. The morphology and structure of these two kinds of δ-MnO_2 were beneficial to the existence of surface hydroxyl groups, which laid a foundation for their excellent adsorption performance.

The EDS characterization and O/Mn ratio of MnO_2 with different crystal forms were shown in Figure 3 and Figure 4. MnO_2 with different crystal forms was mainly composed of Mn and O elements. The content of impurities was lower and had different oxidation degrees. Their size order was as follows: δ_1-MnO_2 > δ_2-MnO_2 > β-MnO_2 > α-MnO_2 > γ-MnO_2 > ε-MnO_2. The higher the O/Mn ratio was, the more abundant the surface oxygen was, and the more unsaturated the oxygen coordination around the manganese vacancy was, resulting in the formation of a large number of hydroxyl groups on the MnO_2 surface, which was more conducive to the surface complexation reaction. Only the oxidation degree (1.99) of β-MnO_2 was close to the standard measurement number of MnO_2 (O/Mn = 2), and the O/Mn ratio of α-MnO_2, γ-MnO_2, and ε-MnO_2 was relatively low. The reasons were as follows: on one hand, the MnO_2 tunnel structure contained impurity cations, in which there were defects and vacancies; on the other hand, EDS analysis only detected the content of surface elements, and some oxygen content of internal structural was not detected. However, the O/Mn ratios of the two different δ-MnO_2 prepared by a hydrothermal method were bigger than 2, indicating that the surface oxygen content of δ-MnO_2 was high and more hydroxyl functional groups could be formed on its surface, so it had the potential to become a high-adsorption adsorbent.

The infrared spectral characteristics of MnO_2 with different crystal forms were analyzed by FT-IR, as shown in Figure 5. The surface hydroxyl stretching vibration peak of α-MnO_2 was at 3407.21 cm^{-1}, surface hydroxyl bending vibration peak was at 1621.88 and 1084.48 cm^{-1}, C bond bending vibration peak was at 1401.33 cm^{-1}, Mn−O lattice vibration characteristic peak was at 594.96 and 514.21 cm^{-1}, and other peaks belonged to the vibration peak of impurities in α-MnO_2. Similarly, β-MnO_2, γ-MnO_2, δ_1-MnO_2, δ_2-MnO_2, and ε-MnO_2 also had surface hydroxyl stretching vibration peaks at 3400 cm^{-1}, surface hydroxyl bending vibration peaks appeared at 1600 and 1100 cm^{-1}, and Mn−O lattice vibration characteristic peaks appeared at 500−600 cm^{-1}. Among them, δ_1-MnO_2 prepared by manganese acetate had C−O and C−H vibration peaks of acetate ions at 1400 cm^{-1}. The vibration peaks of hydroxyl groups on the surface of β-MnO_2, γ-MnO_2, and ε-MnO_2 were weak, so the relative content of hydroxyl groups was less. However, δ_1-MnO_2 and δ_2-MnO_2 had wide and strong hydroxyl vibration peaks, and the surface hydroxyl on them was rich, which was more conducive to the surface complex reaction with heavy metal ions; the excellent adsorption effect would be achieved.

3.2. Effect of MnO_2 Crystal Form on Equi-Acidity Point pHs. Each MnO_2 had a characteristic equi-acidity point pHs. When MnO_2 was mixed into the electrolyte, the pH value of the electrolyte changed toward the equi-acidity point pHs, which was related to the complexation reaction of hydroxyl groups on

https://doi.org/10.1021/acsomega.1c06939
ACS Omega 2022, 7, 9602−9613

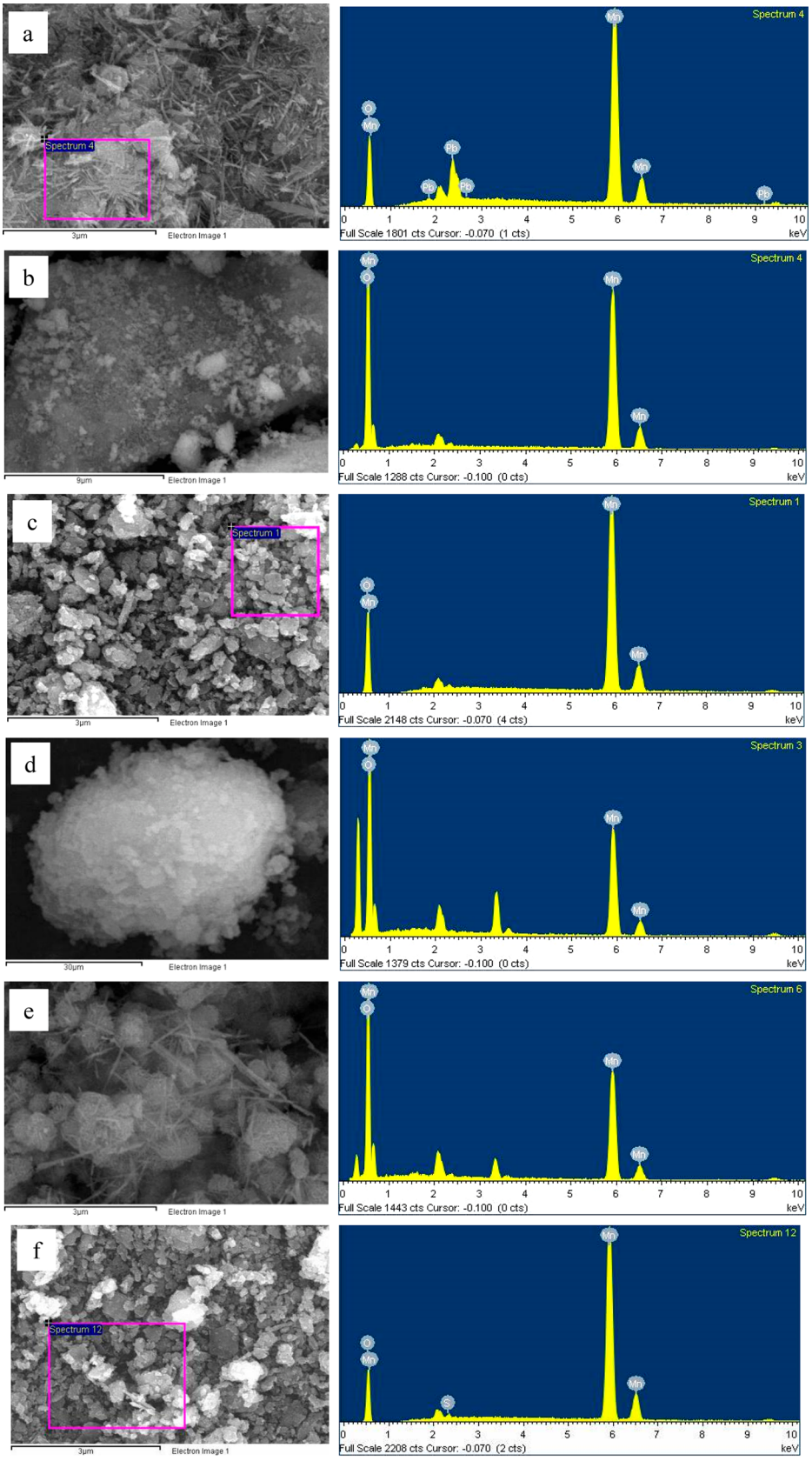

Figure 3. EDS images of MnO_2 with different crystal forms (a, α-MnO_2; b, β-MnO_2; c, γ-MnO_2; d, δ_1-MnO_2; e, δ_2-MnO_2; f, ε-MnO_2).

the surface of MnO_2. The equi-acidity point pH values of MnO_2 with different crystal structures were determined in $MnSO_4$ solution; the results are as shown in Figure 6. The pH curves were plotted with the initial pH of $MnSO_4$ solution before the reaction as the abscissa and the final pH of $MnSO_4$ solution after the reaction as the ordinate. The intersection point of these

https://doi.org/10.1021/acsomega.1c06939
ACS Omega 2022, 7, 9602−9613

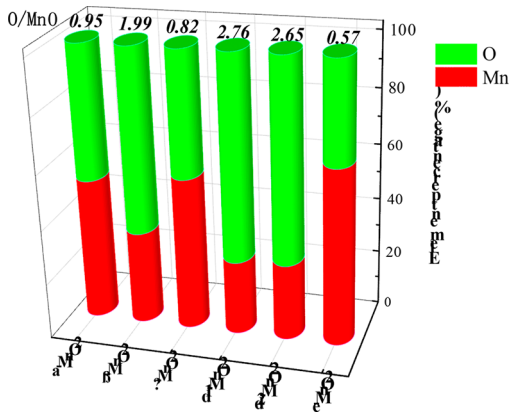

Figure 4. O/Mn ratio of MnO_2 with different crystal forms.

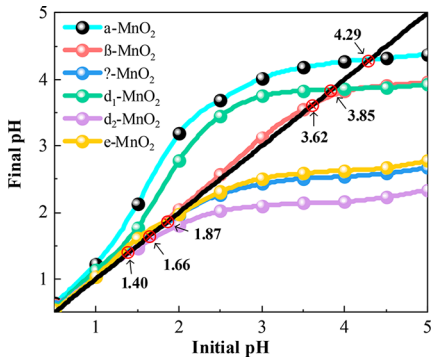

Figure 6. Equi-acidity point pH of MnO_2 with different crystal forms.

curves and the straight line $y = x$ were the equi-acidity point pHs of the various MnO_2's, respectively.[22]

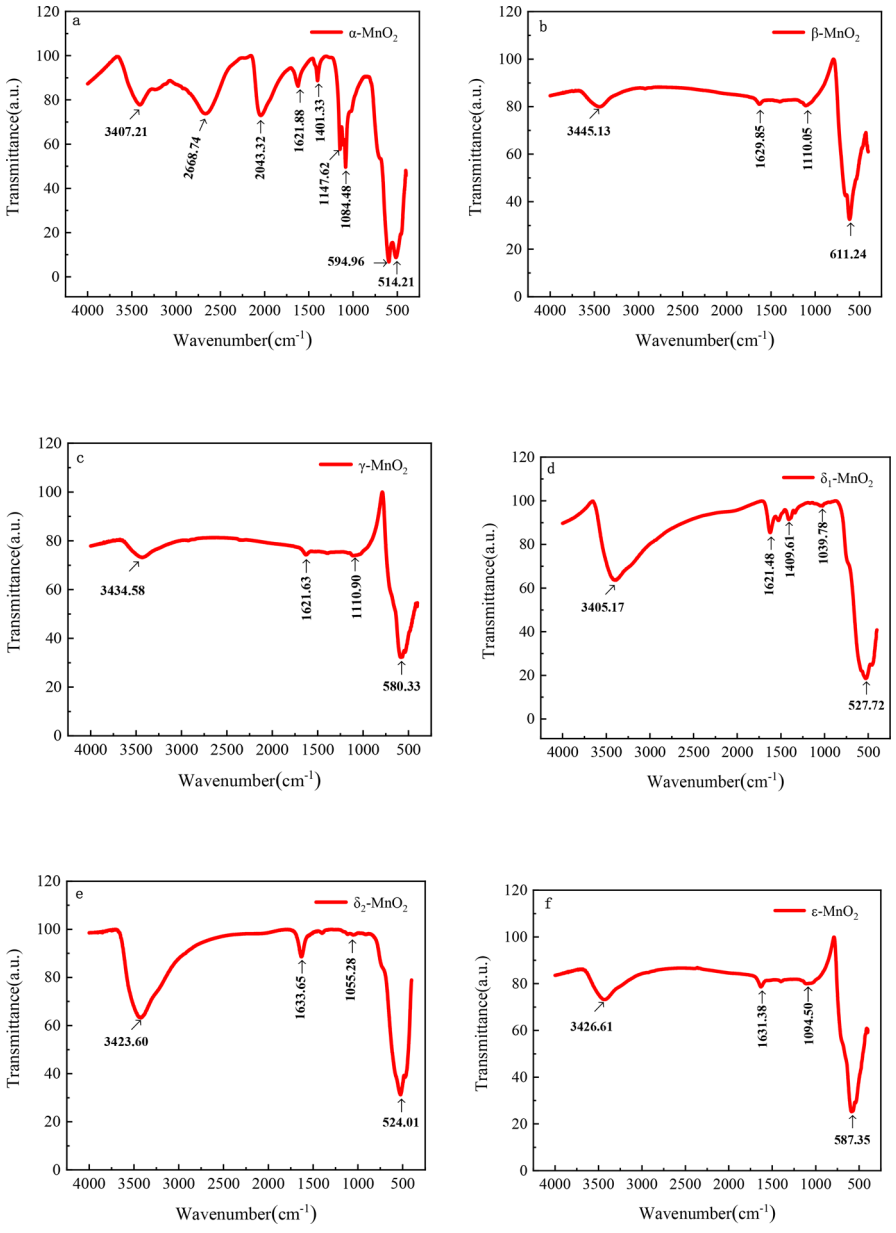

Figure 5. FT-IR analysis of MnO_2 with different crystal forms (a, α-MnO_2; b, β-MnO_2; c, γ-MnO_2; d, δ_1-MnO_2; e, δ_2-MnO_2; f, ε-MnO_2).

https://doi.org/10.1021/acsomega.1c06939
ACS Omega 2022, 7, 9602−9613

It could be seen from Figure 6 that the equi-acidity point pH of MnO_2 with different crystal forms was different. That of α-MnO_2 was the highest, reaching 4.29. The second was δ_1-MnO_2 and β- MnO_2, 3.85 and 3.62, respectively. The equi-acidity point pHs of ε-MnO_2, γ-MnO_2, and δ_2-MnO_2 were relatively low, 1.87, 1.66, and 1.40, respectively. Wang Jinliang et al. believed that the equi-acidity point pHs of MnO_2 obtained by different methods were different, mainly because the amounts of the surface acid hydroxyl and basic hydroxyl were unequal. When these two hydroxyl groups adsorbed metal cations, they release H^+ and OH^-, which acted as a buffer for electrolyte solution. The more acidic the hydroxyl groups were, the more cations adsorbed, and the lower the equi-acidity point pH was.[22,23] The authors believed that this view had some limitations, and the principle of the surface complexation reaction could better explain the reasons for the similarities and differences of equi-acidity point pHs. The protonation reaction and deprotonation reaction of surface hydroxyl (≡SOH) occurred first when MnO_2 came into contact with solution:[28]

$$\equiv SOH + H^+ \leftrightarrows \equiv SOH_2^+ \quad (2)$$

$$\equiv SOH(+OH^-) \leftrightarrows \equiv SOH^- + H^+(+H_2O) \quad (3)$$

Surface complexation reaction would produce and adsorb metal ions in solution on these surface structures, usually involving one or more surface structures, but the desorption reaction would occur when the H^+ concentration was too high. With Mn^{2+} as an example, the reaction was as follows:[29,30]

$$\equiv SOH + Mn^{2+} \leftrightarrows \equiv SOMn^+ + H^+ \quad (4)$$

$$\equiv SOH_2^+ + Mn^{2+} \leftrightarrows \equiv SOMn^+ + 2H^+ \quad (5)$$

$$\equiv SO^- + Mn^{2+} + H_2O \leftrightarrows \equiv SOMnOH + H^+ \quad (6)$$

At the same time, because the complexing ability of hydroxyl groups on the MnO_2 surface to different cations was different, the ion exchange reaction still existed on the surface of MnO_2:[31]

$$\equiv SONa + Mn^{2+} = \equiv SOMn^+ + Na^+ \quad (7)$$

When the pH of the electrolyte solution was higher than the equi-acidity point pH of MnO_2, the surface hydroxyl groups of MnO_2 would undergo deprotonation reaction and be complexed with metal ions to release H^+, which reduced the pH of electrolyte solution. When the pH of the solution was lower than the equi-acidity point pH of MnO_2, the surface hydroxyl group mainly underwent protonation reaction and consumed H^+, which increasesd the pH. The equi-acidity points of MnO_2 were essentially the equilibrium pH value of adsorption and desorption between surface hydroxyl and metal ions. The high or low of the equi-acidity point pH depended on the amount of surface hydroxyl and the size of the complexation ability.

3.3. Effect of Reaction Conditions on Equi-Acidity Point pH. Among several manganese dioxides, the equi-acidity point pH of β-MnO_2 was 3.62, which was in a relatively central position. In order to obtain the influence law of reaction conditions on equi-acidity point pH, it was studied and reported on in this section. The electrolyte was the $MnSO_4$ solution. When the reaction temperature was 20, 30, 50, 70, and 90 °C, the reaction time was 1, 3, 5, 7, and 9 h), and the Mn^{2+} concentration was 5, 15, 30, and 45 g/L, the effect of reaction conditions on the equi-acidity point pH was explored; the results were shown in Figure 7, Figure 8, and Figure 9.

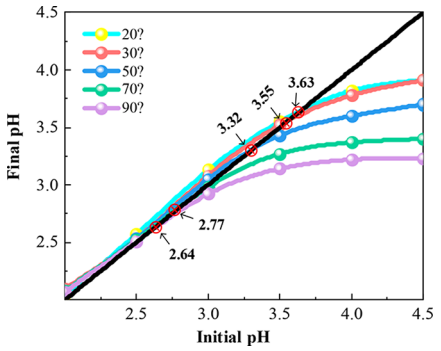

Figure 7. Effect of reaction temperature on equi-acidity point pH.

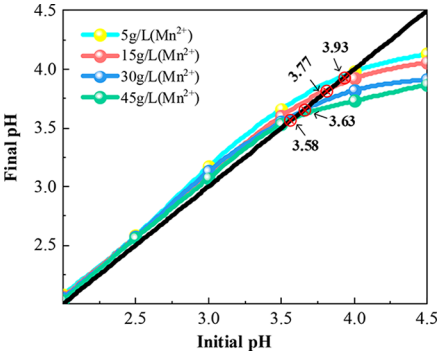

Figure 8. Effect of Mn^{2+} concentration on equi-acidity point pH.

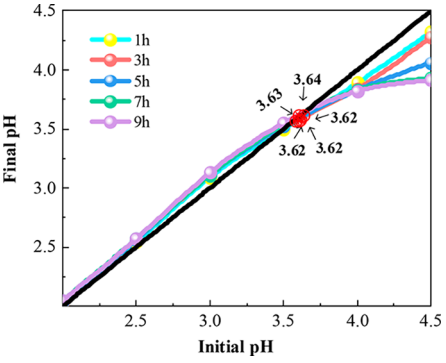

Figure 9. Effect of reaction time on equi-acidity point pH.

It can be seen from Figure 7 that with the increase of temperature, the equi-acidity point pH decreased from 3.63 to 2.64. It can be seen that the complexation reaction between surface hydroxyl groups and metal ions is an endothermic reaction. The complexation reaction between surface hydroxyl and metal ions was reversible according to formula 4. According to Le Chatelier's principle, the reaction would proceed in the direction of reducing heat when the reaction temperature was increased. Therefore, with the increase of reaction temperature, formula 4 proceeded to the right, which could complex more Mn^{2+} and release more H^+, resulting in the decrease of equi-acidity point pH. The equi-acidity point pH decreased with the increase of Mn^{2+} concentration (Figure 8). If a substance in a system was added, the equilibrium system would tend to reduce the reaction direction of this substance according to Le Chatelier's principle. Obviously, formula 4 proceeded to the right with the increase of Mn^{2+} concentration. So, equi-acidity point pH decreased with the increase of Mn^{2+} concentration. It could be found from Figure 9 that the reaction time basically had

https://doi.org/10.1021/acsomega.1c06939
ACS Omega 2022, 7, 9602−9613

no effect on the equi-acidity point pH. However, the increasing or decreasing trend of end-point pH increased gradually with the increase of reaction time, and the end-point pH would not change when the reaction time reached more than 7 h. Therefore, the reaction time could only represent the completion degree of the complexation reaction between surface hydroxyl and metal ions, and would not affect the equi-acidity point pH of MnO_2.

3.4. Relationship between Surface Hydroxyl and Equi-Acidity Points pH. It had been found that the equi-acidity point pH of different MnO_2's varied greatly in the previous experiment. Further explaination was needed regarding the relationship between surface hydroxyl and the equi-acidity point pH, and the change of hydroxyl group in the process of complexation reaction. Although the pH of the equi-acidity point such as α-MnO_2 was highest, it was not considered due to the high impurity content. The δ_1-MnO_2 with the higher equi-acidity point pH, β-MnO_2 with moderate equi-acidity point pH, and δ_2-MnO_2 with lowest equi-acidity point pH were used as the research objects. $MnSO_4$ solutions with pH equaling 0.5 and pH equaling 5 were prepared, and these MnO_2's reacted with $MnSO_4$ solution of two different pHs above. The samples after reaction were analyzed by FT-IR, XPS, and zeta potential, and the results are shown in Figures 10, 11, and 12.

According to previous research, three kinds of MnO_2 (β-MnO_2, δ_1-MnO_2, and δ_2-MnO_2) would decrease the pH of the solution after reacting with a manganese sulfate solution with pH equaling 5, and increase the pH of the solution after reacting with a manganese sulfate solution with pH equaling 0.5. From Figure 10a, it can be seen that after the reaction of β-MnO_2 with a manganese sulfate solution of pH equaling 5, the surface hydroxyl vibration peaks near 3400 and 1100 cm^{-1} disappeared. This was due to the release of H^+ after the complexation of hydroxyl and manganese ions. However, the surface hydroxyl vibration peaks of β-MnO_2 near 3400 and 1100 cm^{-1} were more obvious after reaction with a manganese sulfate solution of pH equaling 0.5. This indicated that the surface hydroxyl of MnO_2 could protonate with H^+ to form more hydroxyl at lower pH. It can be seen from Figure 10b and c that the vibrational peaks of hydroxyl groups on the surface of δ_1-MnO_2 and δ_2-MnO_2 decreased after reacting with a manganese sulfate solution at pH 5. Because δ_1-MnO_2 and δ_2-MnO_2 were rich in surface hydroxyl groups, when the surface hydroxyl group was complexed with manganese ion to release H^+ and reduce the pH to the equi-acidity point pH, the complexation reaction would not occur, and a large number of surface hydroxyl groups remained,. If the pH was increased, the manganese ions would continue to be complexed. In this way, the surface hydroxyl groups were expected to complex more manganese ions, thus greatly increasing the adsorption effect of MnO_2. Similarly, the hydroxyl vibration peaks on the surface of δ_1-MnO_2 and δ_2-MnO_2 were enhanced after reaction with manganese sulfate solution with pH equaling 0.5. The surface hydroxyl bending vibration peak of δ_1-MnO_2 appeared at 1097.81 cm^{-1}; the C-bond heteropeak near 1400 cm^{-1} was replaced by H^+, which increased the number of surface hydroxyls.

The chemical composition and atomic valence of MnO_2 surface elements could be analyzed by XPS. The XPS full spectra, O 1s spectra, and Mn 2p spectra before and after the reaction of δ_1-MnO_2 and δ_2-MnO_2 were shown in Figure 11.

From the XPS full pattern, it can be seen that the two kinds of MnO_2 were mainly composed of Mn and O before the reaction, and there was a small amount of K^+ and C pollution. The K^+

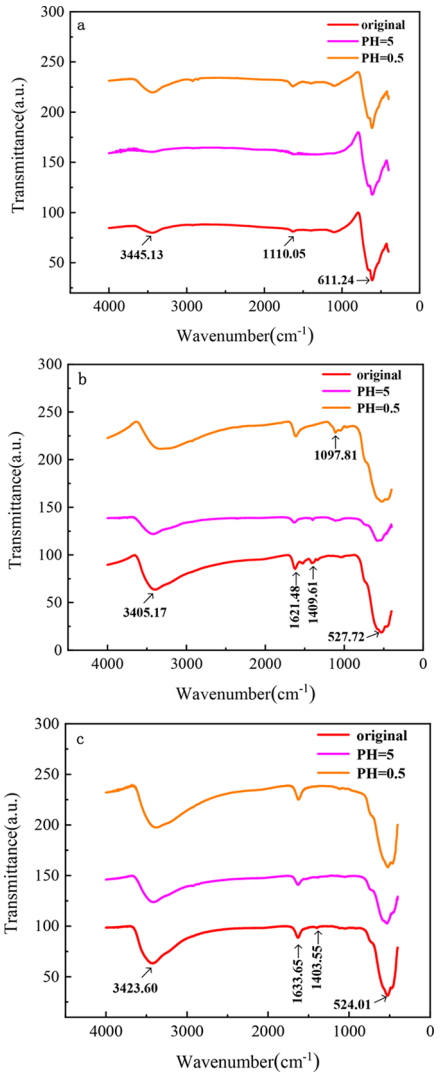

Figure 10. FT-IR spectra of MnO_2 after reaction with manganese sulfate solution (a, β-MnO_2; b, δ_1-MnO_2; c, δ_2-MnO_2).

peak of the two kinds of MnO_2 after the reaction disappeared; the reasons were as follows. The surface hydroxyl of δ_2-MnO_2 complexed a large amount of Mn^{2+}, which underwent ion exchange reaction with K^+, and H^+ on the surface of MnO_2 would substitute K^+ at low pH. The C peak of δ_1-MnO_2 weakened after the reaction; the reason was also the same, which was a desorption process. It could be found from Figure 11b that the O 1s peaks of the two MnO_2 were asymmetric; the structural oxygen (Mn−O) near 529.9 mV and the adsorbed oxygen (Mn−OH) near 530.94 mV could be obtained by software fitting, indicating that there were a large number of hydroxyl functional groups on the surfaces of the two MnO_2.[32] After the reaction of δ_1-MnO_2 and δ_2-MnO_2, the O 1s peak moved to the right, indicating that the bond energy of the O 1s peak increased, the adsorption oxygen content increased, and the surface hydroxyl was more abundant. This was because H^+ around δ_1-MnO_2 replaced C and K^+ adsorbed on its surface and the protonation of surface hydroxyl groups at low pH. However, the surface hydroxyl of δ_2-MnO_2 did not decrease but rather increased, which may be due to the fact that the hydroxyl consumed by the complexation reaction was less than the adsorbed water on the MnO_2. It can be found from the Mn 2p spectrum that the peaks of Mn $2p_{3/2}$ and Mn $2p_{1/2}$ appeared at

https://doi.org/10.1021/acsomega.1c06939
ACS Omega 2022, 7, 9602−9613

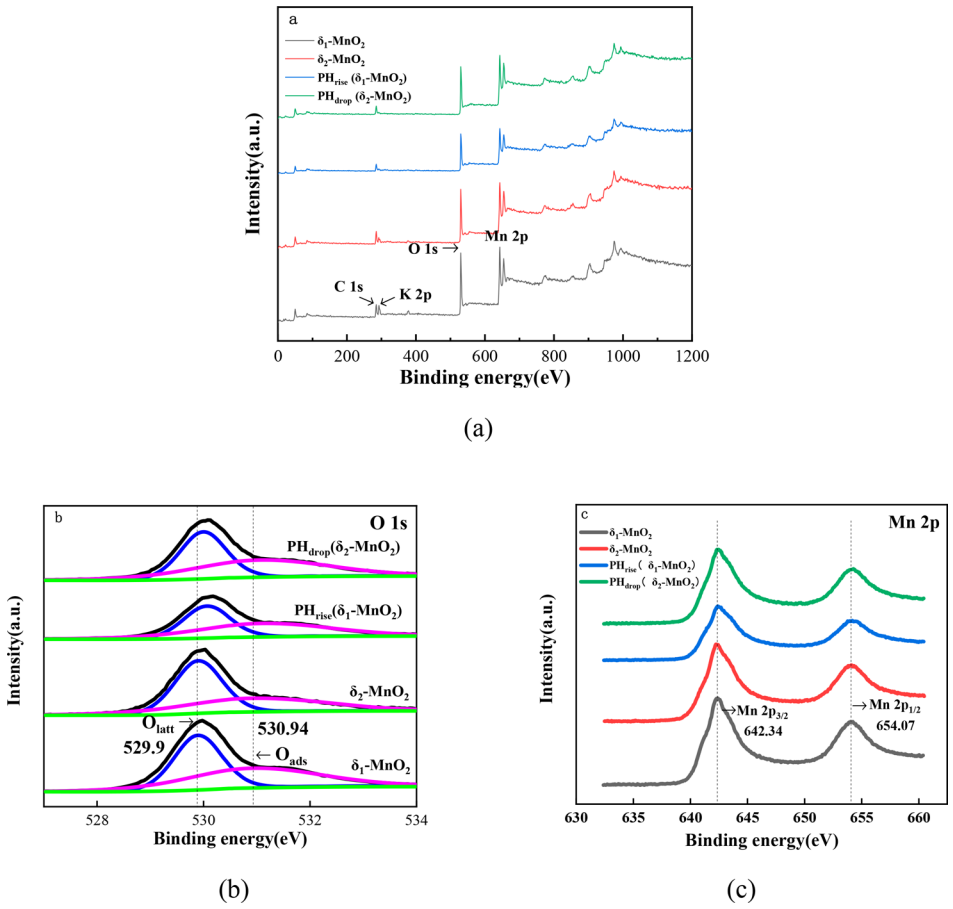

Figure 11. XPS spectra of δ_1-MnO_2 and δ_2-MnO_2 before and after reaction (a, XPS full spectra; b, O 1s spectra; c, Mn 2p spectra).

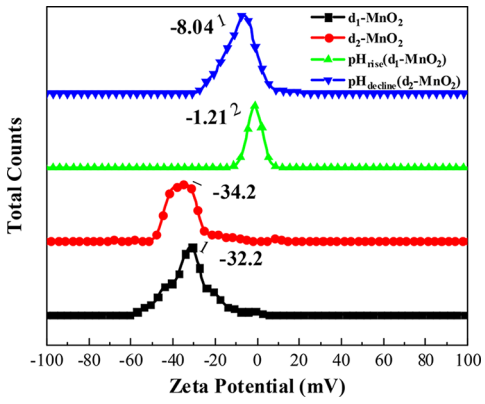

Figure 12. Zeta potential of δ_1-MnO_2 and δ_2-MnO_2 before and after reaction.

the bond energies of 642.34 mV and 654.07 mV, indicating that manganese elements in the two kinds of MnO_2 were basically in the form of Mn^{4+}. The surface hydroxyl complexation reaction was a microreaction, so there was no significant difference in the bond energy before and after the reaction.

The zeta potential was generated by the diffused electric double layer, which was formed because the surface charge of the particle attracted the surrounding anti-signal ions. The charged situation on the surface of the MnO_2 particle can be understood according to its zeta potential value. The zeta potential in this experiment was measured in water with pH = 7, as shown in Figure 12. From Figure 12, the zeta potential values of the two MnO_2 were −32.2 mV and −34.2 mV before the reaction, respectively, which was due to the formation of $\equiv SO^-$ by surface hydroxyl deprotonation. The zeta potential values of the two MnO_2 increased to −1.21 mV and −8.04 mV after the reaction, but the reasons were different. The main reason for the increase of δ_1-MnO_2 zeta potential was that the surface hydroxyl reacted with H^+ to form part of $\equiv SOH_2^+$ under acidic conditions, which hindered the deprotonation of surface hydroxyl.

The reason for the increase of δ_2-MnO_2 was that hydroxyl reacts with metal ions to form ≡SOMnOH on the surface of particles, which separated most of the hydroxyl and made it not deprotonated. The zeta potential changes of the two kinds of MnO_2 were caused by the complexation of surface hydroxyl groups, which further showed that the surface hydroxyl groups played a decisive role in the equi-acidity point pH of MnO_2.

3.5. Adsorption of Co^{2+} and Ni^{2+} in $MnSO_4$ by MnO_2.

Previous studies on MnO_2 found that the change of equi-acidity point pH was mainly caused by surface hydroxyl complexation. MnO_2 with abundant surface hydroxyl groups still had the most hydroxyl groups and did not participate in the reaction; this was mainly because the hydroxyl complexation changed the pH of the solution, so that the reaction could not continue. Therefore, repeatedly adjusting and controlling pH was expected to improve the adsorption performance of MnO_2.[33] In this paper, the adsorption of heavy metals Co^{2+} and Ni^{2+} in high-concentration $MnSO_4$ solution was attempted by using the characteristic of MnO_2.

https://doi.org/10.1021/acsomega.1c06939
ACS Omega 2022, 7, 9602−9613

3.5.1. MnO_2 Adsorption Method for Co^{2+} and Ni^{2+} in $MnSO_4$. The adsorption of six kinds of MnO_2 and the effect of pH adjustment times on δ-MnO_2 adsorption efficiency were shown in Figure 13.

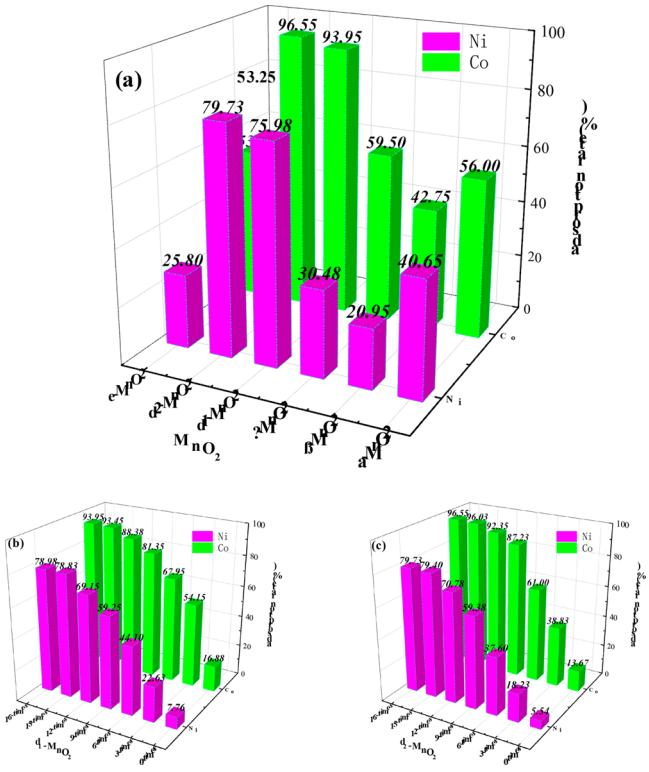

Figure 13. Adsorption of CO^{2+} and Ni^{2+} by MnO_2. (a) Adsorption rates of Co^{2+} and Ni^{2+}. (b) Effect of pH adjustment times on δ_1-MnO_2 adsorption efficiency. (c) Effect of pH adjustment times on δ_2-MnO_2 adsorption efficiency.

It can be seen from Figure 13a that two kinds of δ-MnO_2 with rich surface hydroxyl groups had high adsorption capacity, especially δ_2-MnO_2 for Co^{2+} and Ni^{2+} with adsorption rate reaching 96.55% and 79.73%, respectively. The adsorption rate of MnO_2 with fewer surface hydroxyl groups was relatively low, for example, the adsorption rates of β-MnO_2 for Co^{2+} and Ni^{2+} were only 20.95% and 42.75%. The adsorption rate of MnO_2 for Co^{2+} was slightly higher than that of Ni^{2+}, indicating that MnO_2 had a stronger adsorption capacity for Co^{2+}, and the surface hydroxyl group could better complex Co^{2+}. It could be found from Figure 13b and c that only a small amount of Co^{2+} and Ni^{2+} were adsorbed by the two δ-MnO_2 without adjusting the pH of the solution. With the increase of pH adjustment times, the adsorption capacity increased continuously. When the adjustment times reached 16 times, the pH of the solution no longer decreased, and the adsorption rate tended to be stable, indicating that the adsorption capacity on the surface of MnO_2 reached saturation.

Figure 14 showed the adsorption process of Co^{2+} and Ni^{2+} by MnO_2 in $MnSO_4$ solution. First, MnO_2 particles with surface hydroxyl groups entered into $MnSO_4$ solution. The complexation reaction between surface hydroxyl and metal ions made the pH of the solution decrease continuously. When the pH dropped to a certain value, the reaction was not going on. At this time, some Mn^{2+} and a small amount of Co^{2+} and Ni^{2+} were adsorbed. When the pH of the $MnSO_4$ solution was adjusted to

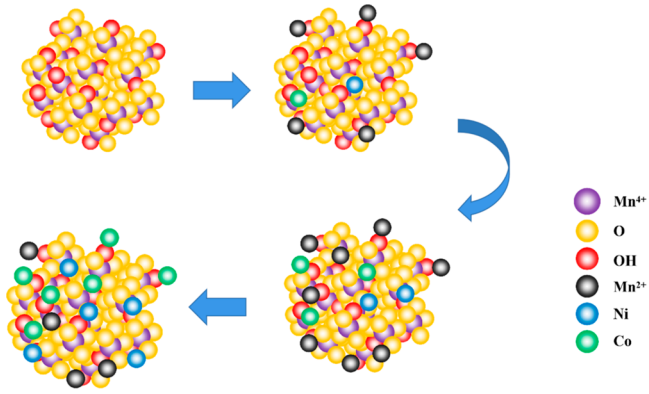

Figure 14. Adsorption process of Co^{2+} and Ni^{2+} in $MnSO_4$ solution by MnO_2.

return to the initial value, the complexation reaction would continue again, and the pH would also decrease. By repeatedly adjusting the pH of the solution, more Mn^{2+}, Co^{2+}, and Ni^{2+} were adsorbed, and the amount of hydroxyl complex sites on the surface was gradually increased. At the same time, Mn^{2+} and Co^{2+}, which were more easily complexed by hydroxyl groups, would undergo ion exchange reaction with Mn^{2+},[34] which increased the adsorption amount of Co^{2+} and Ni^{2+}. When the hydroxyl sites on the surface were all occupied, the pH of $MnSO_4$ solution did not change and the adsorption reached saturation.

3.5.2. Effect of MnO_2 Dosage on Adsorption Performance. The concentration of Mn^{2+} was 20 g/L, Co^{2+} was 80 mg/L, and Ni^{2+} was 80 mg/L, the reaction time was 60 min, the reaction temperature was 80 °C, the pH value was controlled at 7, and the dosage of MnO_2 was 1, 5, 10, 15, and 20 g/L, respectively. The adsorption rate of Co^{2+} and Ni^{2+} in manganese sulfate solution by δ-MnO_2 with different amounts of added MnO_2 was shown in Figure 15.

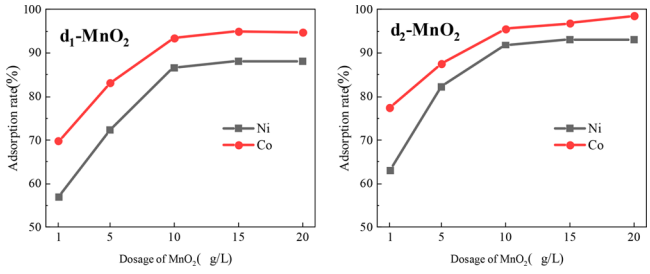

Figure 15. Effect of δ-MnO_2 dosage on adsorption of Co^{2+} and Ni^{2+}.

It could be seen from Figure 15 that the adsorption rate of δ-MnO_2 for Co^{2+} and Ni^{2+} in manganese sulfate solution increases with the increase of addition amount. The adsorption of Co^{2+} and Ni^{2+} by δ_1-MnO_2 and δ_2-MnO_2 reached a high value when the dosage was 1 g/L. Since the surface adsorption MnO_2 addition, the surface adsorption point energy was fully utilized. With the increase of MnO_2 addition, the total adsorption point increased, the adsorption probability of Co^{2+} and Ni^{2+} increased, and the utilization rate of adsorption point decreased.[35] When the addition amount increased to 10 g/L, the adsorption rate of Co^{2+} and Ni^{2+} reached the maximum basically, and the effect of increasing MnO_2 addition was not obvious, which may be caused by the competitive adsorption between manganese dioxide particles.[36] Therefore, a reasonable addition amount was

https://doi.org/10.1021/acsomega.1c06939
ACS Omega 2022, 7, 9602−9613

conducive to the effective utilization of adsorption sites, and the actual production process could be adjusted according to product demand and economic indicators.

3.5.3. Effect of Mn^{2+} Concentration on Adsorption Performance. Co^{2+} concentration was 80 mg/L, Ni^{2+} concentration was 80 mg/L, reaction time was 60 min, reaction temperature was 80 °C, pH value was 7, MnO_2 addition was 10 g/L, and Mn^{2+} concentration was 0, 10, 20, 30, and 40 g/L, respectively. The effect of different Mn^{2+} concentrations on the adsorption of Co^{2+} and Ni^{2+} in manganese sulfate solution by δ-MnO_2 was shown in Figure 16.

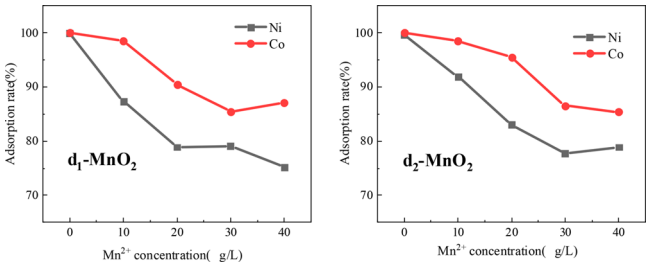

Figure 16. Effect of Mn^{2+} concentration on adsorption of Co^{2+} and Ni^{2+} by δ-MnO_2.

According to Figure 16, it was found that the increase of Mn^{2+} concentration hinders the adsorption of Co^{2+} and Ni^{2+} by δ-MnO_2. When the concentration of Mn^{2+} was 0 g/L, there were only trace amounts of Co^{2+} and Ni^{2+} in the solution, which belongs to a simple water adsorption process. There was no obstruction of Mn^{2+} in the adsorption process. A large number of adsorption sites of MnO_2 were all provided to Co^{2+} and Ni^{2+}, and the adsorption rate of the two ions reached 100%. The higher the concentration of Mn^{2+} in $MnSO_4$ solution, the stronger the inhibition of Co^{2+} and Ni^{2+}, and the lower the adsorption rate. A large number of Mn^{2+} occupies the adsorption sites of MnO_2, and competes with Co^{2+} and Ni^{2+}.[37] When the concentration of Mn^{2+} increased to 30 g/L, the adsorption rate did not change. In the range of low Mn^{2+} concentration, the increase of Mn^{2+} concentration will promote the complexation reaction between Mn^{2+} and surface hydroxyl, and the complexation of Co^{2+} and Ni^{2+} was inhibited. In the range of high Mn^{2+} concentration, the maximum dynamic equilibrium of complexation reaction between manganese dioxide surface and Mn^{2+} was achieved, and the hindrance of Mn^{2+} was not enhanced. Therefore, this adsorption method was suitable for the adsorption of heavy metal ions in high-concentration salt solution.

3.5.4. Characterization of MnO_2 after Adsorption. In order to explore the relationship between MnO_2 adsorption and surface hydroxyl complexation, the δ_2-MnO_2 adsorbed under the optimal conditions (Mn^{2+} concentration of 20 g/L, Co^{2+} concentration of 80 mg/L, Ni^{2+} concentration of 80 mg/L, reaction time of 60 min, reaction temperature of 80 °C, reaction pH value of 7, and MnO_2 addition amount of 10 g/L) was subjected to EDS surface scanning and FT-IR characterization, as shown in Figures 17 and 18.

According to Figure 17, it can be found that there were a large number of Co^{2+} and Ni^{2+} on the surface of the product after δ_2-MnO_2 adsorption, which could well explain that Co^{2+} and Ni^{2+} were adsorbed by MnO_2. At the same time, it could be found that the two ions were mainly distributed on the surface of manganese dioxide particles, and a small amount of them were

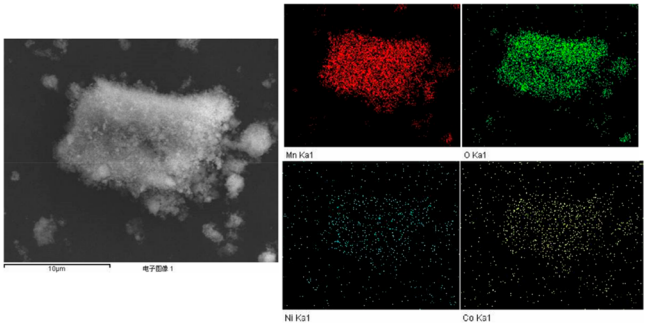

Figure 17. EDS surface scan of δ_2-MnO_2 after adsorption.

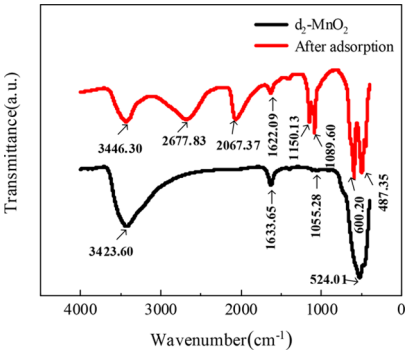

Figure 18. FT-IR spectra of adsorbed δ_2-MnO_2.

evenly distributed in the gap of manganese dioxide particles. It also further shows that the hydroxyl complexation reaction on the surface of manganese dioxide plays a leading role in the adsorption of Co^{2+} and Ni^{2+}.

FT-IR analysis of adsorbed δ_2-MnO_2 was shown in Figure 7. It could be seen that the surface hydroxyl vibration peaks near 3400 and 1600 cm^{-1} were weakened, and new vibration peaks appeared at 2677.83 and 2067.37 cm^{-1}, indicating that Co^{2+} and Ni^{2+} complexed with hydroxyl on the surface of δ_2-MnO_2.[38] The enhancement of vibration peak near 1000 cm^{-1} was due to the increase of adsorbed water on the MnO_2 surface. The vibration peaks of the Mn−O lattice shift and increase near 500−600 cm^{-1}, which was caused by Mn^{2+} adsorption on the δ-MnO_2 surface or Mn_3O_4 and MnOOH generated by reaction.

4. CONCLUSION

In this paper, according to the characteristic of MnO_2 having equi-acidity point pHs, the surface hydroxyl complexation mechanism of MnO_2 was studied, and a new process for MnO_2 to adsorb heavy metals Co^{2+} and Ni^{2+} in high-concentration $MnSO_4$ solution was explored, which provided a method for MnO_2 to adsorb heavy metal ions in high salt solution. Six different types of MnO_2 (α-MnO_2, β-MnO_2, γ-MnO_2, δ_1-MnO_2, δ_2-MnO_2, and ε-MnO_2) were prepared. XRD, SEM, EDS, and FT-IR analysis showed that the morphology and structure of the six types of MnO_2 were quite different. The surface of the two kinds of δ-MnO_2 had defects and a large number of pore structures, their surface oxygen content was high, and the hydroxyl was rich. Using the $MnSO_4$ solution as an electrolyte, the equi-acidity point pH of MnO_2 with different crystal structures was determined. The equi-acidity point pHs of MnO_2 was essentially the equilibrium pH value of adsorption and desorption between surface hydroxyl and metal ions, and the equi-acidity point pH depended on the content of surface

https://doi.org/10.1021/acsomega.1c06939
ACS Omega 2022, 7, 9602−9613

hydroxyl and the complexing ability. Increasing temperature and electrolyte concentration could reduce the equi-acidity point pH, and time had no effect on it. FT-IR, XPS, and ZETA analysis were carried out before and after the reaction of δ-MnO_2. It was verified that the main reason for the change of equi-acidity point pH was the complexation of surface hydroxyl groups, and most of the surface hydroxyl groups of MnO_2 with rich surface were not involved in the reaction. Combined with the equi-acidity point pH characteristics and hydroxyl complexation mechanism, MnO_2 had a good adsorption effect on heavy metals Co^{2+} and Ni^{2+} in high concentration $MnSO_4$ solution by repeatedly controlling pH. The adsorption rates of Co^{2+} and Ni^{2+} could reach 96.55% and 79.73%, respectively. The effects of MnO_2 dosage and Mn^{2+} concentration on the adsorption performance were investigated. The relationship between the surface hydroxyl complexation and the adsorption performance was verified by EDS and FT-IR analysis of the products after MnO_2 adsorption.

AUTHOR INFORMATION

Corresponding Author

Haifeng Wang − *College of Materials and Metallurgy, Guizhou University, Guiyang 550025, China; Guizhou Provincial Key Laboratory of Metallurgical Engineering and Energy Saving, Guiyang 550025, China*; Email: mm.hfwang@163.com

Authors

Mingdong Li − *College of Materials and Metallurgy, Guizhou University, Guiyang 550025, China; Guizhou Provincial Key Laboratory of Metallurgical Engineering and Energy Saving, Guiyang 550025, China*; orcid.org/0000-0002-7883-449X

Jiawei Wang − *College of Materials and Metallurgy, Guizhou University, Guiyang 550025, China; Guizhou Provincial Key Laboratory of Metallurgical Engineering and Energy Saving, Guiyang 550025, China*

Bibo Gou − *College of Materials and Metallurgy, Guizhou University, Guiyang 550025, China; Guizhou Provincial Key Laboratory of Metallurgical Engineering and Energy Saving, Guiyang 550025, China*

Dejin Fu − *College of Materials and Metallurgy, Guizhou University, Guiyang 550025, China; Guizhou Provincial Key Laboratory of Metallurgical Engineering and Energy Saving, Guiyang 550025, China*

Pingyuan Zhao − *College of Materials and Metallurgy, Guizhou University, Guiyang 550025, China; Guizhou Provincial Key Laboratory of Metallurgical Engineering and Energy Saving, Guiyang 550025, China*

Complete contact information is available at: https://pubs.acs.org/10.1021/acsomega.1c06939

Author Contributions

#M.L. and J.W. contributed equally to this work.

Notes

The authors declare no competing financial interest.

ACKNOWLEDGMENTS

The funding supports for this study were obtained from National Natural Science Foundation of China (51764006, 51864012, 51764008); Guizhou Provincial Science Cooperation Program ([2016] 5302, [2017] 5788, [2018] 5781, [2019] 1411, [2019] 2841). The author sincerely thanks the reviewers for their views and suggestions to further improve the quality of the manuscript.

REFERENCES

(1) Liu, X. Y.; Gong, T. C.; Zhang, J.; Ji, J.; Huo, W. C.; Cao, T.; Zhang, Y. X.; Zhang, X.; Liu, Y. Engineering hydrogenated manganese dioxide nanostructures for high-performance supercapacitors[J]. *J. Colloid Interface Sci.* **2019**, *537*, 661−670.

(2) Hua, M.; Zhang, S.; Pan, B.; Zhang, W.; Lv, L.; Zhang, Q. Heavy metal removal from water/wastewater by nanosized metal oxides: A review[J]. *Journal of Hazardous Materials* **2012**, *211*, 317−331.

(3) Zhou, Z.-G.; Du, H.-M.; Dai, Z.; Mu, Y.; Tong, L.-L.; Xing, Q.-J.; Liu, S.-S.; Ao, Z.; Zou, J.-P. Degradation of organic pollutants by peroxymonosulfate activated by MnO_2 with different crystalline structures: Catalytic performances and mechanisms[J]. *Chemical Engineering Journal* **2019**, *374*, 170−180.

(4) Xu, Z.; Yang, W.; Si, W.; Chen, J.; Peng, Y.; Li, J. A novel γ-like MnO_2 catalyst for ozone decomposition in high humidity conditions-[J]. *Journal of Hazardous Materials* **2021**, *420*, 126641.

(5) Ma, J. P.; Ma, Q. Y.; Wang, C.; Zhou, L. J.; Wang, J. J. Research progress on the removal and mechanism of heavy metal ions by manganese dioxide-based nanomaterials [J]. *Environmental chemistry* **2020**, *39* (03), 687−703.

(6) Egorova, A. A.; Bushkova, T. M.; Kolesnik, I. V.; Yapryntsev, A. D.; Kottsov, S. Yu; Baranchikov, A. E. Selective Synthesis of Manganese Dioxide Polymorphs by the Hydrothermal Treatment of Aqueous $KMnO_4$ Solutions[J]. *Russ. J. Inorg. Chem.* **2021**, *66* (2), 141−148.

(7) Dawadi, S.; Gupta, A.; Khatri, M.; Budhathoki, B.; Lamichhane, G.; Parajuli, N. Manganese dioxide nanoparticles: synthesis, application and challenges[J]. *Bulletin of Materials Science* **2020**, *43* (1), 277.

(8) Li, K.; Li, H.; Xiao, T.; Long, J.; Zhang, G.; Li, Y.; Liu, X.; Liang, Z.; Zheng, F.; Zhang, P. Synthesis of manganese dioxide with different morphologies for thallium removal from wastewater[J]. *Journal of Environmental Management* **2019**, *251*, 109563.

(9) Bondar, Y. V.; Alekseev, S. A. Synthesis and evaluation of manganese dioxide with layered structure as an adsorbent for selective removal of strontium ions from aqueous solution[J]. *SN Applied Sciences* **2020**, *2* (8), 1−9.

(10) Wang, X.; Huo, S.; Wang, R.; Wang, H.; Brett, D. J.L.; Ji, S. Synthesis of high surface area mesoporous MnO_2 via a ″metastable″ aqueous interfacial reaction.[J]. *J. Colloid Interface Sci.* **2017**, *503*, 76−85.

(11) Xu, M.; Wang, H.; Lei, D.; Qu, D.; Zhai, Y.; Wang, Y. Removal of Pb(II) from aqueous solution by hydrous manganese dioxide: Adsorption behavior and mechanism[J]. *Journal of Environmental Sciences* **2013**, *25* (3), 479−486.

(12) Peng, L.; Zeng, Q.; Tie, B.; Lei, M.; Yang, J.; Luo, S.; Song, Z. Manganese Dioxide nanosheet suspension: A novel absorbent for Cadmium(II) contamination in waterbody[J]. *J. Colloid Interface Sci.* **2015**, *456*, 108−115.

(13) Meng, K.; Wu, X.; Zhang, X.; Su, S.; Huang, Z.; Min, X.; Liu, Y.'g.; Fang, M. Efficient Adsorption of the Cd(II) and As(V) Using Novel Adsorbent Ferrihydrite Manganese Dioxide Composites.[J]. *ACS omega* **2019**, *4* (20), 18627−18636.

(14) Maneechakr, P.; Mongkollertlop, S. Investigation on adsorption behaviors of heavy metal ions (Cd^{2+}, Cr^{3+}, Hg^{2+} and Pb^{2+}) through low-cost/active manganese dioxide-modified magnetic biochar derived from palm kernel cake residue[J]. *Journal of Environmental Chemical Engineering* **2020**, *8* (6), 104467.

(15) Tao, W. Q.; Lv, R. W.; Tao, Q. Q. Facile Preparation of Novel Manganese Dioxide Modified Nanofiber and Its Uranium Adsorption Performance[J]. *Journal of Applied Mathematics and Physics* **2021**, *09* (07), 1837−1852.

(16) Cheng, M.; Yao, C.; Su, Y.; Liu, J.; Xu, L.; Hou, S. Synthesis of membrane-type graphene oxide immobilized manganese dioxide adsorbent and its adsorption behavior for lithium ion[J]. *Chemosphere* **2021**, *279*, 130487.

(17) Zhang, H.; Xu, F.; Xue, J.; Chen, S.; Wang, J.; Yang, Y. Enhanced removal of heavy metal ions from aqueous solution using manganese

dioxide-loaded biochar: Behavior and mechanism[J]. *Sci. Rep.* **2020**, *10* (1), 6067.
(18) Kozawa, A. Reaction mechanism of hydrogen absorbers made of manganese dioxide[J]. *Electrochemistry and industrial physical chemistry* **1976**, *44* (9), 572−577.
(19) Wu, S.; Xie, F.; Chen, S.; Fu, B. The removal of Pb (II) and Cd (II) with hydrous manganese dioxide: mechanism on zeta potential and adsorption behavior[J]. *Environmental technology* **2020**, *41* (24), 3219.
(20) Haifeng, W.; Xiaoliang, C.; Pingyuan, Z.; Zhaowei, G.; Xiaoyu, Y.; Jiayu, T.; Jiawei, W. Preparation of New Nano-MnO_2 and Its Molybdenum Adsorption in Manganese Sulfate Solution[J]. *Nanoscience and Nanotechnology Letters* **2020**, *12* (9), 1070−1078.
(21) Xia, X. Crystal structure, preparation and discharge performance of manganese dioxide and related manganese oxides (8) [J]. *Battery* **2007**, No. 04, 271−274.
(22) Wang, J. L.; Yu, M.; Li, X. B.; Yan, X. H. Study on pH value of equi-acidity points such as manganese dioxide (I) [J]. *Battery* **1991**, No. 06, 3−6.
(23) Wang, J. L.; Li, X. B.; Yu, M.; Qu, J. Study on pH value of equi-acidity points such as manganese dioxide (II)——pH value of equi-acidity points and Electrochemical Activity of MnO_2 [J]. *Battery* **1992**, No. 05, 195−200.
(24) Xue, W.; Yi, H.; Lu, Y.; Xia, L.; Meng, D.; Song, S.; Li, Y.; Wu, L.; Farias, M. E. Combined electrosorption and chemisorption of As(III) in aqueous solutions with manganese dioxide as the electrode[J]. *Environmental Technology & Innovation* **2021**, *24*, 101832.
(25) Chen, J.; Chen, W.; Huang, M.; Tang, H.; Zhang, J.; Wang, G.; Wang, R. Metal organic frameworks derived manganese dioxide catalyst with abundant chemisorbed oxygen and defects for the efficient removal of gaseous formaldehyde at room temperature[J]. *Appl. Surf. Sci.* **2021**, *565*, 150445.
(26) Bischoff, C. F.; Fitz, O. S.; Burns, J.; Bauer, M.; Gentischer, H.; Birke, K. P.; Henning, H.-M.; Biro, D. Revealing the Local pH Value Changes of Acidic Aqueous Zinc Ion Batteries with a Manganese Dioxide Electrode during Cycling[J]. *J. Electrochem. Soc.* **2020**, *167* (2), 020545.
(27) Wei, C.; Xu, C.; Li, B.; Du, H.; Kang, F. Preparation and characterization of manganese dioxides with nano-sized tunnel structures for zinc ion storage[J]. *J. Phys. Chem. Solids* **2012**, *73* (12), 1487−1491.
(28) Tamura, H.; Oda, T.; Nagayama, M.; Furuichi, R. Acid-Base Dissociation of Surface Hydroxyl Groups on Manganese Dioxide in Aqueous Solutions[J]. *J. Electrochem. Soc.* **1989**, *136* (10), 2782.
(29) Tang, H. X. Advances in environmental water quality——particle and surface complex (I) [J]. *Progress in environmental science* **1993**, No. 01, 25−41.
(30) Cowley, J. M.; Walkley, A. Reaction between manganous ion and manganese dioxide.[J]. *Nature* **1948**, *161* (4083), 173.
(31) Tang, H. X. Advances in environmental water quality——particle and surface complex (II) [J]. *Progress in environmental science* **1993**, No. 02, 1−13.
(32) Ajith, N.; Bhattacharyya, K.; Ipte, P. R.; Satpati, A. K.; Tripathi, A. K.; Verma, R.; Swain, K. K. Interaction of arsenic(III) and arsenic(V) on manganese dioxide: XPS and electrochemical investigations[J]. *Journal of Environmental Science and Health, Part A* **2019**, *54* (4), 277−285.
(33) Hu, C.-Y.; Kuan, W.-H.; Lee, I-J.; Liu, Y.-J. pH-Dependent mechanisms and kinetics of the removal of acetaminophen by manganese dioxide[J]. *Journal of Environmental Chemical Engineering* **2021**, *9* (2), 105129.
(34) Lefkowitz, J. P.; Elzinga, E. J. Structural alteration of hexagonal birnessite by aqueous Mn(II): Impacts on Ni(II) sorption[J]. *Chem. Geol.* **2017**, *466*, 524−532.
(35) Zhu, W.; Huang, X.; Zhang, Y.; Yin, Z.; Yang, Z.; Yang, W. Renewable molybdate complexes encapsulated in anion exchange resin for selective and durable removal of phosphate[J]. *Chin. Chem. Lett.* **2021**, *32*, 3382−3386.
(36) Zhang, Y.; Tang, Q.; Sun, Y.; Yao, C.; Yang, Z.; Yang, W. Improved utilization of active sites for phosphorus adsorption in FeOOH/anion exchanger nanocomposites via a glycol-solvothermal synthesis strategy[J]. *Journal of Environmental Sciences* **2022**, *111*, 313−323.
(37) Yao, N.; Li, C.; Yu, J.; Xu, Q.; Wei, S.; Tian, Z.; Yang, Z.; Yang, W.; Shen, J. Insight into adsorption of combined antibiotic-heavy metal contaminants on graphene oxide in water[J]. *Sep. Purif. Technol.* **2020**, *236*, 116278.
(38) Yang, Z.; Zhang, Y.; Wang, X.; Tian, Z.; Yang, W.; Graham, N. J.D. Efficient adsorption of four phenolic compounds using a robust nanocomposite fabricated by confining 2D porous organic polymers in 3D anion exchangers[J]. *Chemical Engineering Journal* **2020**, *396*, 125296.

https://doi.org/10.1021/acsomega.1c06939
ACS Omega 2022, 7, 9602−9613